ACS Catalysis

Research Article

pubs.acs.org/acscatalysis

Fischer–Tropsch Synthesis: Influence of Support Incorporation Manner on Metal Dispersion, Metal–Support Interaction, and Activities of Iron Catalysts

Haijun Wan,*,† Baoshan Wu,* Hongwei Xiang, and Yongwang Li

State Key Laboratory of Coal Conversion, Institute of Coal Chemistry, Chinese Academy of Sciences, Taiyuan 030001, People's Republic of China

ABSTRACT: Precipitated Fe/Cu/K Fischer–Tropsch Synthesis (FTS) catalysts incorporated with precipitated and binder Al_2O_3 were characterized by N_2 physical adsorption, Temperature-Programmed Reduction/Desorption (TPR/TPD), and Mössbauer Effect Spectroscopy (MES). It was found that the Al_2O_3 incorporation manner plays an important role on metal dispersion and metal–support interaction, which dramatically influence the H_2/CO adsorption, reduction, and carburization, as well as FTS performances of iron catalysts. Specifically, the incorporation of Al_2O_3 during precipitation (i.e., precipitated Al_2O_3) leads to high Fe_2O_3 dispersion and strengthens the Fe–Cu and Fe–K contacts, which in turn promote the reduction and increase the surface basic sites as well as H_2 and CO adsorptions. In sharp contrast, Al_2O_3 added either after precipitation or after heat treatment of the iron precursor (i.e., binder Al_2O_3) is likely to form a strong metal–support interaction (i.e., Fe–Al_2O_3 interaction) and decrease the surface basicity, thereby inhibiting CO adsorption. Correspondingly, in slurry-phase FTS reaction, it was observed that the addition of precipitated Al_2O_3 facilitates catalyst carburization and improves the FTS activity. As expected with the presence of binder Al_2O_3, the reduced catalysts contain small amounts of iron carbides and show low FTS activity as well as water gas shift (WGS) reactivity. Further, presumably because of more basic sites than binder Al_2O_3 supported catalysts, the catalyst incorporated with precipitated Al_2O_3 shows lower selectivity to light hydrocarbons (methane, C_2–C_4, C_5–C_{11}, and C_{12}–C_{18}) but remarkably higher selectivity to heavy hydrocarbons (C_{19}^+). These observations were explained in terms of the influence of the Al_2O_3 incorporation manner on the promotional effects of Cu and K.

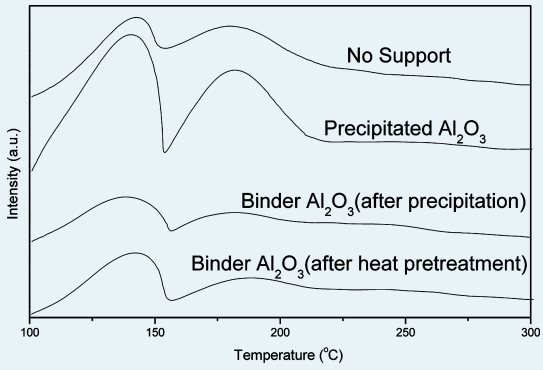

KEYWORDS: *Fischer–Tropsch synthesis, iron catalyst, precipitated Al_2O_3, binder Al_2O_3, metal dispersion, metal-support interaction*

1. INTRODUCTION

Fischer–Tropsch Synthesis (FTS) aimed at converting synthesis gas to transportation fuels has attracted much attention in recent years because of the diminishing fossil fuel resources.[1,2] The advantages of iron FTS catalyst compared to other metals (e.g., cobalt and ruthenium) include its low cost, reversible water gas shift (WGS) reactivity, and low methane selectivity.[3,4] Al_2O_3 and SiO_2 are normally employed as supports in iron catalyst to stabilize catalyst crystallites from sintering and provide robust frame to keep the catalyst away from structure breakage during FTS reaction, especially in slurry-phase continuously stirred tank reactor (CSTR).[5−7] However, unfortunately, the addition of support suppresses the reduction and carburization of the catalyst, and causes low FTS activity, mainly stemming from the strong metal–support interaction.[8−10]

To improve the structural properties of iron catalysts without sacrificing their activity and selectivity, various strategies have been proposed to optimize the support effect, including incorporation of support in various manners, optimization of support content, and modification of support.[11−13] Dlamini et al.[14] investigated the effect of SiO_2 incorporation manner (e.g., precipitated and binder SiO_2) on precipitated Fe/Cu/K catalyst, and found that the catalyst with precipitated SiO_2 contains smaller amounts of iron carbides, resulting in lower CO conversion. The observations were attributed to the strong metal–support interaction, which inhibits catalyst reduction and carburization. Yang et al.[15] studied the influence of SiO_2 content on Fe/Mn/K catalysts, and showed that the catalyst activity decreases with the addition of higher levels of SiO_2. Further, the authors also investigated the effect of SiO_2 incorporation manner (i.e., precipitated and binder SiO_2), and found that the catalyst incorporated with precipitated SiO_2 exhibits stronger metal–support interaction, inhibiting catalyst reduction and carburization. However, in FTS reaction, the addition of precipitated SiO_2 leads to higher activity and lower selectivity to gaseous hydrocarbons, presumably because of the higher effective K content. Recently, Qing et al.[16] modified Fe-SiO_2 interaction with zirconia and found that the Fe-SiO_2 interaction can be weakened by the incorporation of zirconia.

Received: November 11, 2011
Revised: July 17, 2012
Published: July 24, 2012

Table 1. Details of the Catalyst Samples Used in This Study

	catalyst composition (in parts by weight)		
catalysts	nominal	analyzed	Al_2O_3 addition
CA-0	100Fe/6Cu/5K	100Fe/6.4Cu/4.7K	no Al_2O_3 added
CA-1	100Fe/6Cu/5K/15Al_2O_3	100Fe/6.2Cu/5.4K/14.4Al_2O_3	to the solution mixture prior to precipitation (named precipitated Al_2O_3)
CA-2	100Fe/6Cu/5K/15Al_2O_3	100Fe/6.2Cu/4.7K/14.4Al_2O_3	after precipitation (named binder Al_2O_3)
CA-3	100Fe/6Cu/5K/15Al_2O_3	100Fe/6.1Cu/4.4K/13.4Al_2O_3	after spray-drying at 200 °C (named binder Al_2O_3)

The optimum activity and selectivity toward C_5^+ hydrocarbons were observed on the catalyst with the zirconia loading of 100Fe/20ZrO_2.

Although numerous studies of SiO_2 effect on Fe/Cu/K catalyst have been reported in literature, there is no clear picture of Al_2O_3 effects on metal dispersion and metal−support interaction as well as Cu and K promotions. Further, given that support can promote the dispersion of the catalyst crystallites and increase the number of exposed metal sites,[17] the optimization of synergistic effects of support on metal dispersion and metal−support interaction could provide a basis for exploring novel iron FTS catalyst with excellent performance in terms of activity, selectivity, and stability. Herein, we prepared a series of Fe/Cu/K/Al_2O_3 catalysts with different Al_2O_3 incorporation manners, in combination with Temperature-Programmed Reduction/Desorption (TPR/TPD) and Mössbauer Effect Spectroscopy (MES) characterization technologies, to elucidate the roles of metal dispersion and metal−support interaction on catalyst surface basicity, reduction, and carburization as well as FTS performances. It is anticipated that the approach described here is useful in the development and selection of optimum FTS catalysts for generating valuable hydrocarbons.

2. EXPERIMENTAL SECTION

2.1. Catalyst Preparation. The catalysts were prepared by the precipitation method. A solution containing $Fe(NO_3)_3$ (99.9+%, Taiyuan Chemical Co., P.R. China) and $Cu(NO_3)_2$ (99.9+%, Taiyuan Chemical Co., P.R. China) with weight ratio of 100Fe/6Cu was precipitated at 80 °C using Na_2CO_3 (99.9+%, Taiyuan Chemical Co., P.R. China) solution. After filtration, the precipitate was mixed with K_2CO_3 (99.9+%, Taiyuan Chemical Co., P.R. China) solution in the amounts required to obtain the desired weight ratio of 100Fe/5K. The alumina gel (30.0% with water as solvent, Taiyuan Chemical Co., P.R. China) was added at different stages during catalyst preparation with weight ratio of 100Fe/15Al_2O_3. Subsequently, the mixture was spray-dried at 200 °C and then calcined at 450 °C for 5 h. Details of the stages at which Al_2O_3 was added and the elemental analysis data of these catalysts are presented in Table 1. These four catalysts were labeled as CA-0, CA-1, CA-2, and CA-3.

2.2. Reaction Setup and Analysis. The FTS reactions were conducted in a 1 L slurry-phase CSTR. For a typical experiment, 20.0 g of catalyst and 320.0 g of liquid paraffin (hydrogenated 1-decene homopolymer, ∼C30 obtained from Taiyuan Chemical Co., P.R. China, boiling point: 346 °C at 1 bar) were charged into the reactor. Subsequently, H_2 and CO were separately metered into the reactor using Brooks 5850E mass flow controllers. The reactor pressure was controlled by a back-pressure regulator. After leaving the reactor, the exit gas passed through a hot trap (120 °C) and a cold trap (0 °C) to collect liquid products. A gas flow totalizer was used to measure the exit gas flow rate. Before FTS reaction, the catalyst was in situ reduced in synthesis gas (H_2/CO = 0.67) at 290 °C, 0.30 MPa and 1000 h^{-1} for 18 h. The gas hourly space velocity (GHSV) is defined as the ratio of the volumes of synthesis gas to the total volumes of catalyst. After in situ reduction, a small amount of reduced catalyst (suspended in the liquid paraffin) was collected from the slurry reactor through a dip tube connected to a sampling trap. To avoid the exposure of the catalyst to air, the sampling system was purged with argon prior to the collection. Subsequently, the samples were tested by Mössbauer to determine the phase compositions. The steady-state reaction conditions were set at 260 °C, 1.5 MPa, H_2/CO = 0.67 and 1000 h^{-1}. The gas and liquid samples were collected at a predetermined time (100 and 200 h). The gas sample was analyzed online by an Agilent 6890N (HP) gas chromatograph (GC) with a 5A molecular sieve column (Ar carrier gas) and an Al_2O_3 column (N_2 carrier gas) equipped with TCD and FID. Oil and wax were analyzed offline using an Agilent 6890N (HP) GC with UA+-(HT) stainless steel capillary column (FID, N_2 carrier gas) and an Agilent 6890N (HP) GC with DB-1 quartz capillary column (FID, N_2 carrier gas), respectively. The carbon balance of the FTS reactions is better than 94 ± 3%.

2.3. Catalyst Characterization. The composition of the catalysts was determined by atomic absorption spectroscopy (AAS) using an Atomscan 16 spectrometer (TJA, U.S.A.).

The Brunauer−Emmett−Teller (BET) surface area, pore volume, and average pore size were tested by N_2 physical adsorption at −196 °C using a Micromeritics ASAP 2500 instrument. The sample was degassed under vacuum at 180 °C for 6 h before measurement.

H_2-TPR experiments were performed in a quartz reactor using a mixture gas of 5% H_2/95% Ar at a flow rate of 50 mL/min. Specifically, 20 mg of catalyst was charged into the quartz reactor. Then the catalyst sample was heated from room temperature to 800 °C at a heating rate of 6 °C/min. The hydrogen consumption rate was monitored by TCD.

H_2, CO and CO_2-TPD experiments were performed with Ar as carrier gas in H_2-TPD and He as carrier gas in CO-TPD as well CO_2-TPD at a flow rate of 50 mL/min. A 200 mg portion of catalyst was charged into the quartz reactor. Note that for H_2 and CO-TPD, the catalyst was first reduced with H_2 at 450 °C or CO at 300 °C for 4 h. In the CO_2-TPD experiments, the catalyst sample was purged with He (50 mL/min) and calcined in situ at 300 °C for 2 h to remove the adsorbed species. Subsequently, the catalyst was reduced in 5% H_2/95% Ar at a flow rate of 50 mL/min for 2 h. In the following steps, H_2, CO, and CO_2 adsorption on catalyst were performed at 100 °C for 30 min, and then the sample was purged with the carrier gas for 30 min to remove the weakly adsorbed species. Subsequently, the TPD was started at a heating rate of 5 °C/min.

The Mössbauer spectra of catalysts were collected at room temperature using a CANBERRA Series 40 MCA constant-acceleration Mössbauer spectrometer (CANBERRA, U.S.A.), using a 25 mCi 57Co in Pd matrix. The spectrometer was

operated in the symmetric constant acceleration mode. The spectra were recorded over 512 channels in mirror image format. Data analysis was performed using a nonlinear least-squares fitting routine that models the spectra as a combination of singlets, quadruple doublets, and magnetic sextuplets based on a Lorentzian line shape profile. The spectral components were identified based on their isomer shift (δ), quadruple splitting (Δ), and magnetic hyperfine field (Hhf). All isomer shift values were reported with respect to metallic iron (α-Fe) at the measurement temperature. Magnetic hyperfine fields were calibrated with the 330 kOe field of α-Fe at ambient temperature.

3. RESULTS AND DISCUSSION

3.1. Textural Properties. The BET surface area and pore size distribution of the catalysts are shown in Table 2 and Figure 1, respectively. Although these supported catalysts contain the same amounts of metal components and Al_2O_3 (as shown in Table 1), the incorporation manner of Al_2O_3 significantly influences the surface area, pore volume, and pore size distribution. As inferred from Table 2 and Figure 1, precipitated Al_2O_3 supported catalyst (CA-1) shows the highest surface area and pore volume as well as the smallest pore size among the tested catalysts, followed by binder Al_2O_3 supported catalysts (CA-3 and CA-2). Lund and Dumesic et al.[10] investigated metal−support interaction with Fe/SiO_2 catalyst, and suggested a model in which Si^{4+} substitutes for Fe^{3+} in the tetrahedral sites near the surface of magnetite. In the case of our study, it is possible that for precipitated Al_2O_3 supported catalyst, Al^{3+} substitutes for a certain amount of Fe^{3+} in the tetrahedral sites, thereby providing a rigid matrix, which helps to prevent complete collapse of the original pore structure during subsequent drying and calcination. Further, the large surface area is also attributed to the fact that precipitated Al_2O_3 leads to high dispersion of Fe_2O_3, which are verified by the later MES studies in section 3.6.

Table 2. Textural Properties of the Fresh Catalysts

catalysts	BET surface area (m^2/g)	pore volume (cm^3/g)	average pore size (nm)
CA-0	21	0.18	33.81
CA-1	114	0.22	7.79
CA-2	48	0.27	24.21
CA-3	86	0.23	10.57

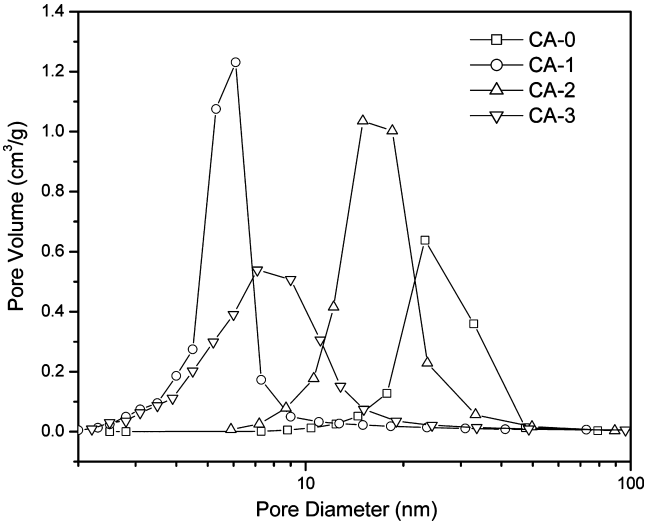

Figure 1. Pore size distribution of the fresh catalysts.

3.2. H_2-TPR. H_2-TPR was used to investigate the effect of the Al_2O_3 incorporation manner on the reduction behavior of iron catalysts. As shown in Figure 2, the reduction process of the catalysts occurs in two stages. The first stage at low temperature is attributed to the transformations of CuO→Cu and Fe_2O_3→Fe_3O_4, whereas the second stage represents the transformation of Fe_3O_4→Fe.[4] For the catalyst incorporated with binder Al_2O_3, there is a small peak at 240 °C in the profiles, which can be attributed to the reduction of CuO to Cu.[13] It is interesting to note that the addition of precipitated Al_2O_3 promotes the reduction of both stages compared to unsupported catalyst, while the addition of binder Al_2O_3 inhibits the reduction of iron catalysts. Given that Cu is a good promoter to facilitate the reduction of iron catalyst,[18] the observed low reduction temperature of precipitated Al_2O_3 supported catalyst may be correlated with the strengthened promotional effect of Cu. One possible explanation is that the precipitated Al_2O_3 facilitates the dispersion of iron crystallites as demonstrated by BET and MES, and therefore enhances the Fe−Cu contact, leading to the increase of Cu promotion effectiveness. However, it is possible that the addition of binder Al_2O_3 forms strong Fe−Al_2O_3 interactions and weakens the Fe−Cu contact, showing the segregation of Cu from Fe. Thus the reduction of the catalysts with binder Al_2O_3 is suppressed.

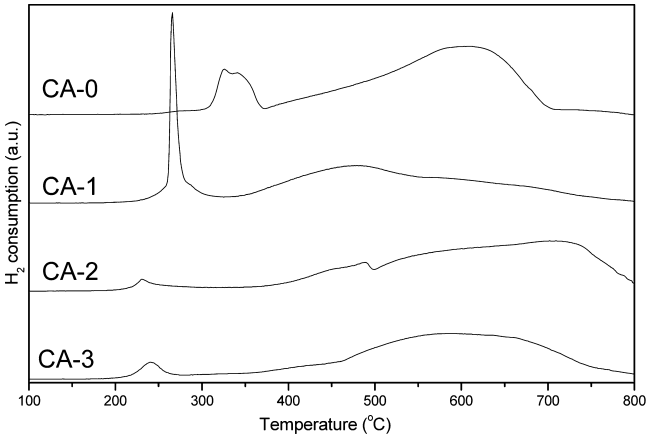

Figure 2. H_2-TPR profiles of the catalysts.

3.3. CO_2-TPD. The effect of Al_2O_3 incorporation manner on the surface basicity of iron catalysts was examined by CO_2-TPD. It was observed that all catalysts show two desorption peaks; one at low temperature corresponding to weak CO_2 adsorption, and the other one at high temperature is ascribed to strong CO_2 adsorption (see Figure 3). Apparently, precipitated Al_2O_3 as support increases the surface basicity while binder Al_2O_3 shows negative effect. Interestingly, though our previous results[11] over precipitated Fe/Al_2O_3 catalyst have shown that the addition of precipitated Al_2O_3 decreases the basic sites because of metal−support interaction, such is not the case in precipitated $Fe/Cu/K/Al_2O_3$ catalyst, implying that precipitated Al_2O_3 affects the surface basicity in an additional way than just forming metal−support interaction.

dx.doi.org/10.1021/cs200584s | ACS Catal. 2012, 2, 1877−1883

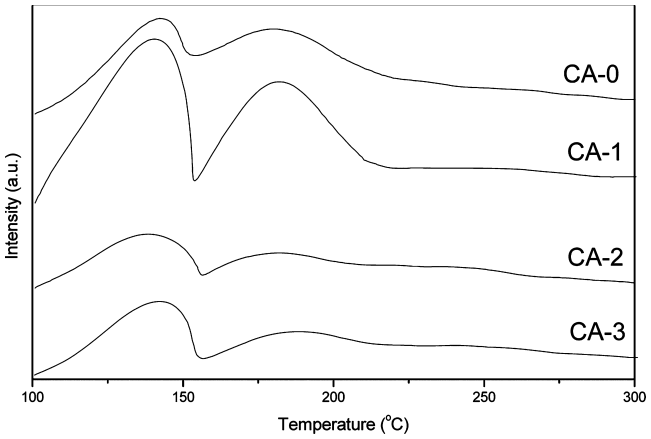

Figure 3. CO_2-TPD profiles of the catalysts.

It is widely accepted that K plays a key role in improving the surface basicity of iron catalyst.[19] Our CO_2-TPD studies reveal that the increased surface basicity of the catalyst with precipitated Al_2O_3 may be attributed to that the addition of precipitated Al_2O_3 favors the high dispersion of Fe_2O_3 and could enhance Fe−K contact, thereby leading to the increase of potassium promotion effectiveness. Further, the addition of precipitated Al_2O_3 is likely to form a weak Fe−Al_2O_3 interaction. As a consequence, the surface basicity of the catalyst is improved. In sharp contrast, for the catalysts incorporated with binder Al_2O_3 (CA-2 and CA-3), the strong Fe−Al_2O_3 interaction and poor dispersion weaken the promotional effect of K displaying weak surface basicity. However, these hypotheses are not proved and must be verified by additional investigations involving bulk phase analysis techniques.

3.4. H_2-TPD. Figure 4 shows the H_2 adsorption behavior of the catalysts. All of the H_2-TPD profiles show a strong peak at

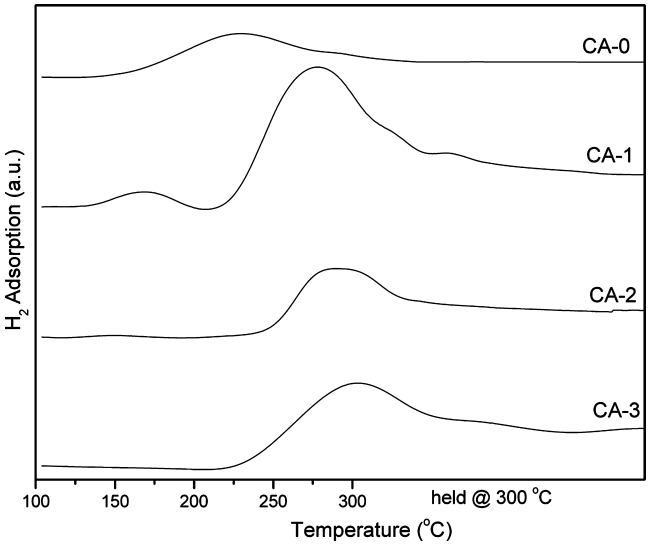

Figure 4. H_2-TPD profiles of the catalysts.

high temperature, attributed to a chemical H_2 adsorption peak. For catalyst CA-1, there is a small adsorption peak at low temperature, which corresponds to weak H_2 desorption in bulk phase. Of the tested catalysts, catalyst CA-1 (incorporated precipitated Al_2O_3) shows the largest amounts of H_2 desorption. Further, the peak areas of all Al_2O_3 supported catalysts are higher than unsupported catalyst (CA-0). It has been reported that Cu as promoter favors H_2 adsorption.[18] It seems plausible that the strong dispersion of precipitated Al_2O_3 enhances the Fe−Cu contact as indicated by H_2-TPR and results in the increase of Cu promotion effectiveness, improving the H_2 adsorption. In contrast, for the catalysts with binder Al_2O_3, the higher surface area should be responsible for the increased H_2 adsorption compared to catalyst CA-0.

3.5. CO-TPD. Additional experiments were performed to investigate the effects of Al_2O_3 incorporation manner on CO adsorption. As shown in Figure 5, it is interesting to note that

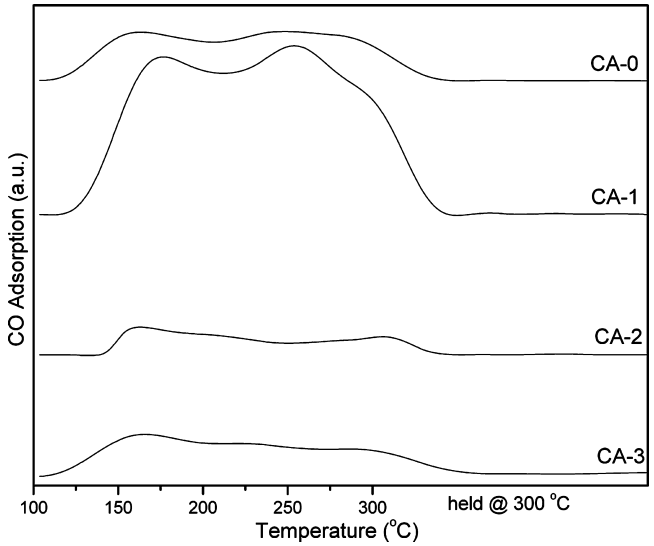

Figure 5. CO-TPD profiles of the catalysts.

the addition of precipitated Al_2O_3 significantly improves the CO adsorption, while the addition of binder Al_2O_3 suppresses the CO adsorption. Miller et al.[20] reported that the extent of CO adsorption increases with the increasing K level. Kölbel[21] investigated the effect of K on precipitated Fe/Cu/SiO_2 catalyst, and also found that the addition of K promoter increases CO chemisorption. In our CO-TPD profiles, the increased CO adsorption on the catalyst incorporated with precipitated Al_2O_3 is therefore attributed to the enhanced promotional effect of K. For the catalysts incorporated with binder Al_2O_3 (CA-2 and CA-3), the strong metal−support interaction decreases the effective potassium content and inhibits CO adsorption. The results are in good agreement with CO_2-TPD.

3.6. Bulk Phase Structure of Tested Catalysts. The phase compositions of the fresh catalysts were determined by MES analyses. Figure 6 shows the Mössbauer spectra of the fresh catalysts. Table 3 lists the iron-phase composition of the fresh catalysts, as determined by fitting the Mössbauer spectra. As shown by Table 3, the catalyst with precipitated Al_2O_3 (CA-1) shows larger amounts of superparamagnetic Fe^{3+} than these with binder Al_2O_3 (CA-2 and CA-3), indicating that the crystallite size of catalyst CA-1 is smaller than other catalysts. These results further confirm that the addition of precipitated Al_2O_3 leads to the higher Fe_2O_3 dispersion than binder Al_2O_3. Note that, although most of the published results report[15] higher than 50% superparamagnetic fraction of the Fe, such is not the case in this study. Given that all the catalysts were prepared by spray-dried technology, the dehydration rate

dx.doi.org/10.1021/cs200584s | ACS Catal. 2012, 2, 1877−1883

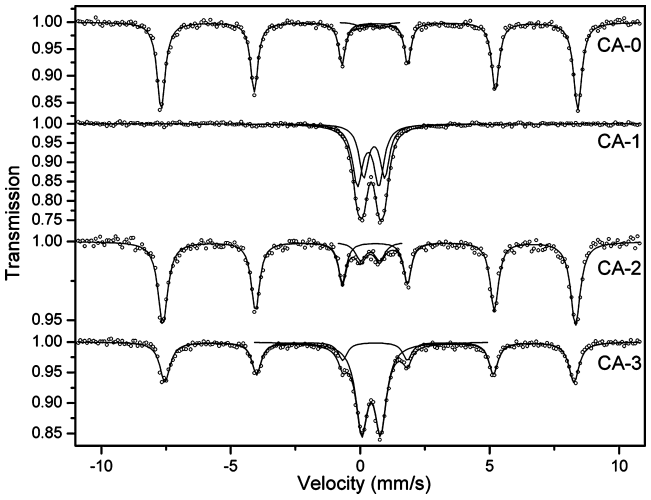

Figure 6. Mössbauer spectra of the fresh catalysts.

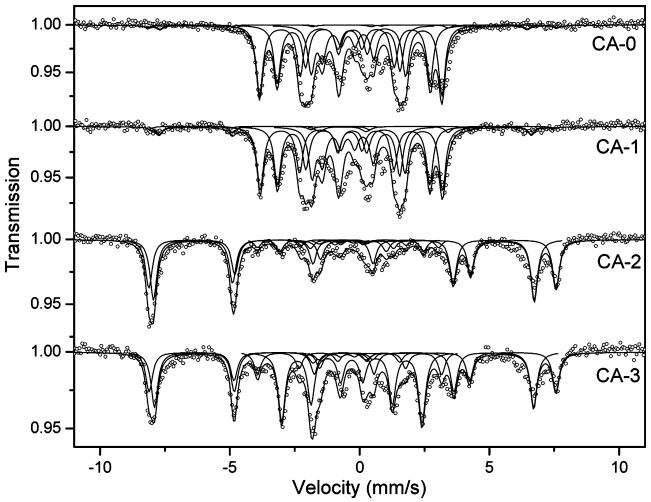

Figure 7. Mössbauer spectra of the reduced catalysts.

Table 3. Mössbauer Spectra Parameters of the Fresh Catalysts

		MES parameters			
catalysts	phases	IS (mm/s)	QS (mm/s)	Hhf (kOe)	area (%)
CA-0	α-Fe_2O_3	0.46	−0.21	500	98.6
	α-Fe_2O_3 (spm)	0.35	0.80		1.4
CA-1	α-Fe_2O_3 (spm)	0.31	0.83		55.3
	α-Fe_2O_3 (spm)	0.54	0.81		44.7
CA-2	α-Fe_2O_3	0.46	−0.22	496	90.3
	α-Fe_2O_3 (spm)	0.47	0.69		9.7
CA-3	α-Fe_2O_3	0.47	−0.22	491	47.0
	α-Fe_2O_3 (spm)	0.42	0.73		53.0

Table 4. Mössbauer Spectra Parameters of the Reduced Catalysts[a]

		MES parameters			
catalysts	phases	IS (mm/s)	QS (mm/s)	Hhf (kOe)	area (%)
CA-0	Fe_3O_4 (A)	0.35	0.14	490	2.4
	Fe_3O_4 (B)	0.65	0.06	440	3.3
	χ-Fe_5C_2	0.30	−0.08	218	39.1
		0.30	0.29	106	25.3
	ε'-$Fe_{2.2}C$	0.30	0.14	173	27.9
	Fe^{2+}	0.65	1.80		2.0
CA-1	Fe_3O_4 (A)	0.35	0.14	482	0.9
	Fe_3O_4 (B)	0.65	0.19	446	4.6
	χ-Fe_5C_2	0.30	−0.04	218	34.8
		0.30	0.31	105	26.6
	ε'-$Fe_{2.2}C$	0.30	0.14	182	31.5
	Fe^{2+}	0.65	1.80		1.7
CA-2	Fe_3O_4 (A)	0.27	−0.01	488	34.2
	Fe_3O_4 (B)	0.62	0.04	456	42.7
	χ-Fe_5C_2	0.33	−0.22	217	5.7
		0.30	−0.63	104	5.1
	ε'-$Fe_{2.2}C$	0.30	−0.01	172	8.6
	Fe^{2+}	0.65	1.80		2.0
	Fe^{3+}	0.35	0.80		1.5
CA-3	Fe_3O_4 (A)	0.29	0.03	487	19.5
	Fe_3O_4 (B)	0.60	0.00	454	27.2
	χ-Fe_5C_2	0.33	−0.11	220	11.1
		0.30	0.33	104	4.9
	ε'-$Fe_{2.2}C$	0.30	0.01	168	34.8
	Fe^{2+}	0.65	1.80		2.5

[a]Reduction conditions: 290 °C, 0.3 MPa, H_2/CO = 0.67 and GHSV = 1000 h^{-1}.

during spray drying is faster than that in the normal drying process, probably leading to the greatly aggregated porous Fe_2O_3/FeOOH framework and thereby the large catalyst crystals.

The Mössbauer data for the reduced catalysts is used to determine the phase compositions of reduced iron catalysts, which would allow us to compare the effects of Al_2O_3 incorporation manner on catalyst reduction as well as the initial activities of these catalysts. Figure 7 shows the Mössbauer spectra of the reduced catalysts. Table 4 lists the iron-phase composition of the catalysts, as determined by fitting the Mössbauer spectra. As shown by Table 4, the amounts of iron carbides on precipitated Al_2O_3 supported catalyst (CA-1) are the highest among the tested catalysts, followed by unsupported catalyst and binder Al_2O_3 supported catalysts. It is clear that the addition of precipitated Al_2O_3 facilitates the carburization of iron catalyst, while the addition of binder Al_2O_3 (either after precipitated or heat treatment) suppresses carburization.

As shown by CO_2 and CO adsorption, the addition of precipitated Al_2O_3 facilitates the high dispersion of the catalyst and may significantly increase the effectiveness of K promotion, improving CO adsorption. In the reduction process, the enhanced CO adsorption promotes the introduction of C and thus facilitates the carburization of the catalyst. When binder Al_2O_3 is incorporated into the catalyst, the strong metal−support interaction reduces the promotion effectiveness of K and thus inhibits iron carburization. In addition, a stronger metal−support interaction probably exists on the catalyst (CA-2) with binder Al_2O_3 added after precipitation than that after heat treatment (CA-3), resulting in lower amounts of iron carbides. These observations further strengthen the hypothesis that the addition of precipitated Al_2O_3 leads to an increase of K promotion effectiveness, whereas the strong metal−support interaction in binder Al_2O_3 supported catalysts causes the reduction of K effectiveness.

3.7. FTS Performances. The effects of Al_2O_3 incorporation manner on CO conversion are shown in Table 5. It is interesting to note that the incorporation of precipitated Al_2O_3

dx.doi.org/10.1021/cs200584s | ACS Catal. 2012, 2, 1877−1883

Table 5. Effects of Incorporation Manner of Al_2O_3 on Catalyst Activity and Selectivity[a]

	catalysts							
	CA-0		CA-1		CA-2		CA-3	
	time on stream/h							
	99	195	96	195	99	197	98	197
CO conversion/%	82.2	82.4	91.4	91.1	14.7	15.7	17.4	17.0
H_2 conversion/%	71.2	72.9	80.0	79.9	25.3	27.0	32.4	31.2
H_2+CO conversion/%	77.8	78.6	86.8	85.9	18.9	20.2	23.4	22.7
exit molar H_2/CO ratio	1.10	1.00	1.43	1.33	0.58	0.58	0.55	0.55
extent of WGS/(P_{H2}·P_{co_2}/P_{co}·P_{H2O})	116.3	104.6	110.8	100.9	0.4	0.5	0.5	0.5
	Hydrocarbon Selectivities/wt %							
CH_4	4.0	4.2	4.5	4.2	7.0	6.9	15.3	16.0
C_{2-4}	5.1	5.5	5.4	5.6	9.5	9.4	18.3	17.9
C_{5-11}	21.9	22.9	23.2	22.5	38.4	39.6	32.9	32.6
C_{12-18}	24.0	26.5	26.4	26.5	39.5	39.0	32.1	32.0
C_{19}^+	45.0	41.0	40.6	41.2	5.6	5.1	1.5	1.5
CO conversion to CO_2/mol %	46.1	45.8	43.8	45.5	23.7	23.4	25.0	26.1

[a]Reaction conditions: 260 °C, 1.5 MPa, H_2/CO = 0.67, and GHSV = 1000 h^{-1}.

as support increases the catalyst activity while the addition of binder Al_2O_3 displays a negative effect. As indicated by MES results, there is a clear correlation between the carburization extent and the catalytic activity; the higher carburization extent in the catalyst the higher CO conversion. As shown by H_2 and CO adsorption results, the addition of precipitated Al_2O_3 not only favors the CO adsorption but also improves the H_2 adsorption, thereby leading to the high FTS activity. Correspondingly, as expected in the presence of binder Al_2O_3, the reduced catalysts contain small amounts of iron carbides, which suppress CO adsorption and cause low FTS activity. It is also possible that with the addition of binder Al_2O_3, the catalysts CA-2 and CA-3 show an out layer of Al_2O_3 which suppresses H_2 and CO adsorptions (see Figure 5), hence decreasing catalytic conversion. However, these hypotheses must be verified by additional investigations involving surface analysis techniques.

It is well-known that a reversible water-gas shift (WGS) reaction accompanies the FTS reaction over iron catalyst.[12] The Q_{WGS} value represents equilibrium of WGS reaction and is usually used to measure WGS activity.[22] It was observed that, of the tested catalysts, the Q_{WGS} value of unsupported catalyst is the highest, followed by the catalyst with precipitated Al_2O_3 (see Table 5). In contrast, the Q_{WGS} values of the catalysts with binder Al_2O_3 are much lower than other catalysts, indicating that precipitated Al_2O_3 slightly decreases WGS reactivity, whereas WGS reaction is dramatically suppressed by the addition of binder Al_2O_3. In addition, it was observed that the H_2/CO exit ratio is lower than 2.0 for all the catalysts. Note that the H_2/CO inlet ratio is only 0.67 in our current study. Further, in the case of unsupported and precipitated Al_2O_3 supported catalysts, though CO conversion is higher than 80%, near 45% CO was converted to CO_2 (see Table 5) through WGS reaction. In other words, 45% H_2 was generated on these two catalysts. Hence, the low H_2/CO inlet ratio and high WGS activity should account for the low H_2/CO exit ratio, particularly with these highly active catalysts (CA-0 and CA-1).

Product distribution of the catalysts is shown in Table 5. Note that catalyst CA-3 shows the highest selectivity toward gaseous (methane, C_2−C_4) and light hydrocarbons (C_5−C_{11} and C_{12}−C_{18}) but the lowest selectivity toward heavy hydrocarbons (C_{19}^+), followed by catalyst CA-2. Interestingly, the addition of precipitated Al_2O_3 shifts the selectivity toward heavy hydrocarbons (C_{19}^+). Although the starkly different catalyst reactivities make it difficult to compare the product selectivity, the higher selectivity to heavy hydrocarbons (C_{19}^+) with precipitated Al_2O_3 supported catalyst may be attributed to stronger surface basicity compared to binder Al_2O_3 supported catalysts.

4. CONCLUSIONS

The results presented here have provided a better understanding of the effects of Al_2O_3 incorporation manner on the catalytic properties of iron FTS catalyst in terms of H_2/CO adsorption, reduction, and carburization as well as FTS performances. Compared to unsupported catalyst, the addition of precipitated Al_2O_3 facilitates the high dispersion of the catalyst crystallites and increases the promotion effectiveness of Cu and K, which in turn significantly promote the reduction and increase the surface basicity of the catalyst. However, the addition of binder Al_2O_3 inhibits the reduction and decreases the surface basicity as well as CO adsorption because of the strong metal−support interaction. As expected in slurry-phase FTS reaction, the addition of precipitated Al_2O_3 facilitates carburization of iron catalyst and increases the FTS activity as well as product selectivity toward C_{19}^+ hydrocarbons. In contrast, the addition of binder Al_2O_3 probably causes the reduction of K promotion effectiveness and dramatically suppresses catalyst carburization, thereby decreasing the FTS activity and WGS reactivity. For the same reason, the chain growth reaction appears to give way to chain termination reaction on the catalysts incorporated with binder Al_2O_3, resulting in higher selectivity to light hydrocarbons (methane, C_2−C_4, C_5−C_{11}, and C_{12}−C_{18}).

AUTHOR INFORMATION

Corresponding Author

*Phone: +86-351-756-0668. Fax: +86-351-756-0668. E-mail: haijunwan@hotmail.com (H.W.), wbs@sxicc.ac.cn (B.W.).

Present Address

[†]Center for Environmentally Beneficial Catalysis, University of Kansas, Lawrence, Kansas 66047, USA

Funding

This work was supported by the National Outstanding Young Scientists Foundation of China under Contract 20625620 as well as Synfuels CHINA. Co., Ltd.

Notes

The authors declare no competing financial interest.

REFERENCES

(1) Rao, V. S.; Stiegel, G. J.; Cinquergrane, G. J.; Srivastava, R. D. *Fuel Process. Technol.* **1992**, *30*, 83.
(2) Anderson, R. B. *The Fischer−Tropsch Synthesis*; Academic Press: Orlando, FL, 1984.
(3) Jothimurugesan, K.; Goodwin, J. G., Jr.; Santosh, S. K.; Spivey, J. J. *Catal. Today* **2000**, *58*, 335.
(4) Jin, Y.; Datye, A. K. *J. Catal.* **2000**, *196*, 8.
(5) Zhao, R.; Sudsakorn, K.; Goodwin, J. G., Jr.; Jothimurugesan, K.; Gangwal, S. K.; Spivey, J. J. *Catal. Today* **2002**, *71*, 319.
(6) O'Brien, R. J.; Xu, L.; Bao, S.; Raje, A.; Davis, B. H. *Appl. Catal., A* **2000**, *196*, 173.
(7) Sudsakorn, K.; Goodwin, J. G., Jr.; Jothimurugesan, K.; Adeyiga, A. A. *Ind. Eng. Chem. Res.* **2001**, *40*, 4778.
(8) Bukur, D. B.; Lang, X.; Mukesh, D.; Zimmerman, W. H.; Rosynek, M. P.; Li, C. *Ind. Eng. Chem. Res.* **1990**, *29*, 1588.
(9) Zhang, C. H.; Wan, H. J.; Yang, Y.; Xiang, H. W.; Li, Y. W. *Catal. Commun.* **2006**, *7*, 773.
(10) Lund, C. R. F.; Dumesic, J. A. *J. Phys. Chem.* **1981**, *85*, 3175.
(11) Wan, H. J.; Wu, B. S.; Zhang, C. H.; Xiang, H. W.; Li, Y. W.; Xu, B. F.; Yi, F. *Catal. Commun.* **2007**, *8*, 1538.
(12) Zhao, R.; Goodwin, J. G., Jr.; Jothimurugesan, K., Jr.; Gangwal, S. K.; Spivey, J. J. *Ind. Eng. Chem. Res.* **2001**, *40*, 1065.
(13) Bukur, D. B.; Sivaraj, C. *Appl. Catal., A* **2002**, *231*, 201.
(14) Dlamini, H.; Motjope, T.; Joorst, G.; ter Stege, G.; Mdleleni, M. *Catal. Lett.* **2002**, *78*, 1.
(15) Yang, Y.; Xiang, H. W.; Tian, L.; Wang, H.; Zhang, C. H.; Tao, Z. C.; Xu, Y. Y.; Zhong, B.; Li, Y. W. *Appl. Catal., A* **2005**, *284*, 105.
(16) Qing, M.; Yang, Y.; Wu, B.; Xu, J.; Zhang, C.; Gao, P.; Li, Y. *J. Catal.* **2011**, *279*, 111.
(17) Morales, F.; de Groot, F. M. F.; Gijzeman, O. L. J.; Mens, A.; Stephan, O.; Weckhuysen, B. M. *J. Catal.* **2005**, *230*, 310.
(18) Wan, H.; Wu, B.; Zhang, C.; Xiang, H.; Li, Y. *J. Mol. Catal. A* **2008**, *283*, 33.
(19) Zhang, C. H.; Yang, Y.; Teng, B. T.; Li, T. Z.; Zheng, H. Y.; Xiang, H. W.; Li, Y. W. *J. Catal.* **2006**, *237*, 405.
(20) Miller, D. G.; Moskovits, M. *J. Phys. Chem.* **1988**, *92*, 6081.
(21) Kölbel, H. Kalium als struktureller und Energetischer Promotor in Eisenkatalysatoren. In *Actes du Deuxieme Congress International de Catalyse*; Tchnip: Paris, France, 1960; Vol. *II*, p 2075.
(22) Dictor, R. A.; Bell, A. T. *J. Catal.* **1986**, *97*, 121.